JACS
JOURNAL OF THE AMERICAN CHEMICAL SOCIETY
Communication
pubs.acs.org/JACS

Selective Formation of Conductive Network by Radical-Induced Oxidation

Jin Young Koo,[†] Yumi Yakiyama,[*,†,⊥] Gil Ryeong Lee,[†] Jinho Lee,[§] Hee Cheul Choi,[‡,§] Yasushi Morita,[∥] and Masaki Kawano[*,†,#]

[†]The Division of Advanced Materials Science, Pohang University of Science and Technology (POSTECH), 77 Cheongam-ro, Namgu, Pohang 790-784, Korea

[‡]Center for Artificial Low Dimensional Electronic Systems, Institute for Basic Science (IBS), 77 Cheongam-ro, Pohang 790-784, Korea

[§]Department of Chemistry, Pohang University of Science and Technology (POSTECH), 77 Cheongam-ro, Namgu, Pohang 790-784, Korea

[∥]Department of Applied Chemistry, Faculty of Engineering, Aichi Institute of Technology, Yachigusa 1247, Yakusa, Toyota 470-0392, Japan

Supporting Information

ABSTRACT: Cd-based coordination networks having channels were formed selectively by using a redox-active aromatic ligand 2,5,8-tri(4-pyridyl)1,3-diazaphenalene (TPDAP, $\mathbf{H^+1^-}$). An electron-conductive network having a $\pi-\pi$ stacking columnar structure of TPDAP formed in the presence of a trace amount of TPDAP radical ($\mathbf{1^\bullet}$). In contrast, a nonconductive network having a dimer unit of $\mathbf{H^+1^-}$ formed in the absence of $\mathbf{1^\bullet}$. These results suggest the presence of a unique oxidation mechanism of TPDAP induced by formation of $\mathbf{H^+1^-}$-$\mathbf{1^\bullet}$ dimer, which was initiated by a trace amount of $\mathbf{1^\bullet}$. The dimerization increased HOMO level of $\mathbf{H^+1^-}$ moiety within the dimer to generate further radicals that could not form when $\mathbf{H^+1^-}$ was well isolated in CH_3OH.

A redox-active porous coordination network[1] can provide a potential-tunable space to achieve numerous benefits, including catalytic activity,[2,3] selective molecular trapping,[4] and tunable electronic/magnetic materials.[5] The redox center of a conventional redox-active network typically consists of metal ions rather than organic ligands. A few redox-active ligands have been synthesized, using mostly TCNQ, TTF, pyrene, or naphthalene diimide skeletons.[6] We prepared various coordination networks based on tripyridyl hexaazaphenalene (TPHAP), which was designed to show the importance of multi-interactivity of the ligand for kinetic network formation.[7] Because TPHAP is not redox-active, we designed another tripyridyl ligand, 2,5,8-tri(4-pyridyl)1,3-diazaphenalene (TPDAP or $\mathbf{H^+1^-}$)[8] to introduce redox activity while keeping the same molecular shape as TPHAP. This change was achieved by replacing nonredox-active central hexaazaphenalene (HAP) with redox-active diazaphenalene (DAP),[9,10] which possesses a higher HOMO level than does HAP. We revealed that $\mathbf{H^+1^-}$ forms a neutral radical ($\mathbf{1^\bullet}$) by one-electron oxidation and can possess two-step redox activity (Figure 1a).[8] Herein we report the selective formation of electron conductive/nonconductive coordination networks of redox-active TPDAP (Figure 1b). We also report an unexpected

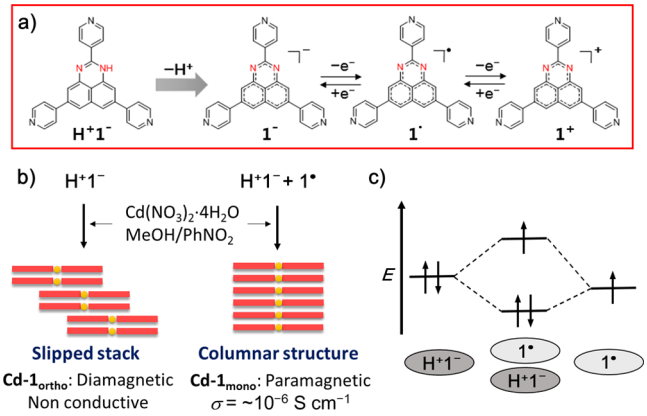

Figure 1. Features of TPDAP. (a) TPDAP two-step redox activity. (b) Schematic model of selective network formation based on redox active ligand $\mathbf{H^+1^-}$. (c) $\mathbf{H^+1^-}$-$\mathbf{1^\bullet}$ dimer formation and HOMO increase.

oxidation mechanism of TPDAP in CH_3OH; this mechanism can be initiated by a trace of $\mathbf{1^\bullet}$ during the network formation process (Figure 1c). The experimental results suggested the formation of $\mathbf{1^\bullet\cdots H^+1^-}$ π-dimer, which caused further oxidation of $\mathbf{H^+1^-}$ by increasing its HOMO level. Meanwhile, $\mathbf{H^+1^-}$ was never oxidized in CH_3OH in the absence of $\mathbf{1^\bullet}$ because no dimer formation occurred.

Because $\mathbf{H^+1^-}$ has much higher HOMO level than does TPHAP (+1.8 eV) the surface of $\mathbf{H^+1^-}$ oxidizes readily under ambient conditions.[8] The surface oxidation of $\mathbf{H^+1^-}$ crystals was monitored by solid-state electron spin resonance (ESR); a broad ESR signal (g = 2.004) was observed immediately after the crystals were exposed to air. The ESR signal intensity gradually increased and reached an asymptote within 72 h in air and within 36 h during purging with O_2 gas (Figure S2). During the process, the crystal color changed from red to dark red and gave a $\mathbf{1^\bullet-1^\bullet}$ dimer peak in ESI-MS; the conclusion is that TPDAP radical $\mathbf{1^\bullet}$

Received: November 25, 2015
Published: January 27, 2016

DOI: 10.1021/jacs.5b12355
J. Am. Chem. Soc. 2016, 138, 1776−1779

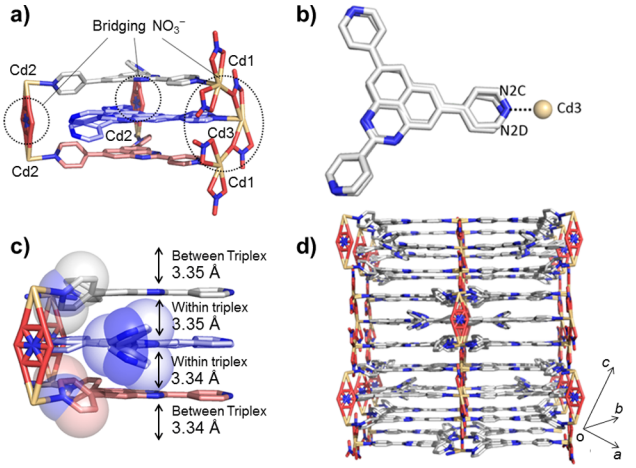

Figure 2. Crystal structures of **Cd-1**$_{mono}$ network. (a) Structure of main triplex unit: bidentate $\mathbf{H^+1^-}$ (top, gray), bidentate $\mathbf{1^-}$ (bottom, pale red), and disordered group (middle, pale blue) of monodentate $\mathbf{H^+1^-}$. (b) Disordered TPDAP model in the middle part of the triplex. The occupancy factor of the Cd3 atom is 0.39. (c) The $\pi-\pi$ stacking distances of central DAP skeleton along the columnar axis. (d) One-dimensional columnar structure. Blue, N; yellow, Cd; red, O. Hydrogen atoms are omitted for clarity.

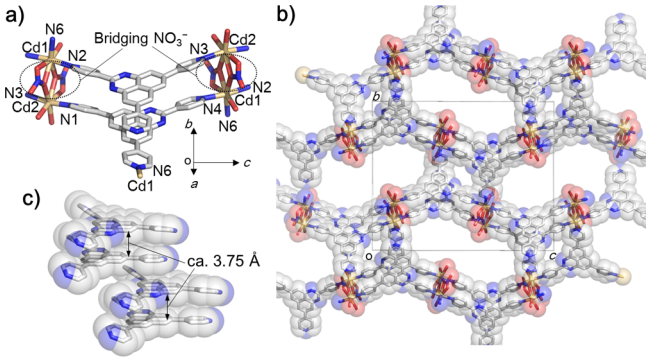

Figure 3. Crystal structures of the **Cd-1**$_{ortho}$ network. (a) Structure of main dimer unit of **Cd-1**$_{ortho}$. (b) Interpenetrated 2D zigzag sheet structure of **Cd-1**$_{ortho}$. (c) Slip-stacked structure in **Cd-1**$_{ortho}$. Intramolecular $\pi-\pi$ stacking distances of the DAP skeleton in the dimer structure were 3.75 Å. Gray, C; blue, N; yellow, Cd; red, O. Hydrogen atoms are omitted for clarity.

was generated by surface oxidation of $\mathbf{H^+1^-}$ crystal (Figures S3 and S4). A quantitative analysis of the spin amount of oxidized crystals ($\mathbf{1_{ox}}$) using TEMPO as a reference indicated that 0.06% of the total $\mathbf{H^+1^-}$ was oxidized (Table S1). In addition, ESR signal intensity of $\mathbf{1_{ox}}$ increased when the sample was cooled from 315 to 105 K (Figure S5). This trend can be attributed to improvement of spin alignment as temperature decreases and to the absence of significant spin−spin interaction within radicals. FT-IR measurement of $\mathbf{1_{ox}}$ gave almost the same spectrum as that of $\mathbf{H^+1^-}$ (Figure S6).

We prepared redox active coordination networks having channels using TPDAP and Cd^{2+}. We found significant structural differences depending on the presence/absence of $\mathbf{1^\bullet}$. The $\mathbf{1_{ox}}$ powder produced a dark red block crystal of ESR active network, $[Cd_{2.39}(NO_3^-)_{3.8}(\mathbf{H^+1^-})_2(\mathbf{1^-})(H_2O)_{6.95}(CH_3OH)_{1.5}]$ (**Cd-1**$_{mono}$; monoclinic $P2/n$) obtained by layering diffusion of a CH_3OH solution of $Cd(NO_3)_2{\cdot}4H_2O$ into a CH_3OH−nitrobenzene solution of $\mathbf{1_{ox}}$ in air at 20 ± 1 °C for 1 d (Figures 2, S7, and S8). As a control experiment, we confirmed that, instead of using $\mathbf{1_{ox}}$, **Cd-1**$_{mono}$ could be obtained from the CH_3OH solution of $\mathbf{H^+1^-}$ and $\mathbf{1^\bullet}$ ($\mathbf{H^+1^-}$:$\mathbf{1^\bullet}$ = 10:1) generated by oxidation of a CH_3OH solution of $\mathbf{H^+1^-}$ by PbO_2.[8] This is further evidence that the surface oxidized product is $\mathbf{1^\bullet}$. The network contained a triplex of three ligands as a main unit in which three Cd^{2+} centers are bridged by two NO_3^- (Figure 2a).

The triplex consisted of bidentate $\mathbf{H^+1^-}$ (top), bidentate $\mathbf{1^-}$ (bottom), a disordered group (middle) of monodentate $\mathbf{H^+1^-}$, and a trace of radical $\mathbf{1^\bullet}$. The disorder of monodentate $\mathbf{H^+1^-}$ (middle) coordinates to a partially occupied Cd3 ion with the occupancy factor of 0.39, which is determined by both the X-ray and ICP analyses (Figure 2b, Table S2). As a result, the monodentate $\mathbf{H^+1^-}$ formed $\pi-\pi$ interactions between two central DAP skeletons within the triplex (Figure 2c). Although we could not identify $\mathbf{1^\bullet}$ by X-ray analysis because of its scarcity (3.26×10^{-6} mmol in 0.658 mg of **Cd-1**$_{mono}$ estimated by ESR (Table S3)), the results of electron conductivity measurement of a single crystal suggest that $\mathbf{1^\bullet}$ can intercalate in the columnar structure (*vide infra*). The assembly of the triplexes formed a porous columnar structure with the pore size of 5.5 Å × 5.2 Å (Figures 2d and S9b). The averaged $\pi-\pi$ stacking distance of the central DAP skeleton in the columnar structure was 3.3 Å, which is shorter by 0.2 Å than that in an $\mathbf{H^+1^-}$ crystal (Figure 2c). On the basis of the total number of radicals in $\mathbf{1_{ox}}$, a non-negligible increase in the spin occurred in **Cd-1**$_{mono}$ (Table S4). The results of ESR and UV−vis spectroscopic experiments (*vide infra*) indicate that oxidation occurred to produce further $\mathbf{1^\bullet}$ in the solution during crystallization.

In contrast, the layering diffusion of a CH_3OH solution of $Cd(NO_3)_2{\cdot}4H_2O$ into a CH_3OH−nitrobenzene solution of nonoxidized $\mathbf{H^+1^-}$ solid in air at 20 ± 1 °C for 1 d yielded a single crystal of nonconductive, ESR-silent network, $[Cd_2(NO_3^-)_4(\mathbf{H^+1^-})_2(H_2O)_2(CH_3OH)_5]$ (**Cd-1**$_{ortho}$; orthorhombic $P22_12_1$; Figures 3 and S8). X-ray single crystal structure analysis revealed a network structure formed by interpenetrated 2D zigzag sheets composed of TPDAP dimer units bridged by four Cd^{2+} ions in pentagonal bipyramidal geometry (Figures 3a and S10). These Cd^{2+} ions were coordinated by bridging NO_3^- ions, $\mathbf{H^+1^-}$, and water molecules. This network had pores with the size of 20.1 Å × 7.3 Å in which solvent molecules (CH_3OH, H_2O, or nitrobenzene) were encapsulated (Figures 3b and S9a). However, it was difficult to make models of solvent molecules because of the severe disorder within the pore. Each $\mathbf{H^+1^-}$ in **Cd-1**$_{ortho}$ was stacked with a large overlap of DAP skeletons within the dimer unit, but $\pi-\pi$ interaction between the dimer units was absent (Figure 3c).

The redox property of network crystals of **Cd-1**$_{mono}$ and of **Cd-1**$_{ortho}$ were evaluated by solid-state cyclic voltammetry (CV) using a Pt working electrode. We detected reversible two-step redox waves (Figure S11). Previously, solid-state CV of $\mathbf{H^+1^-}$ crystals showed two reversible redox waves that correspond to $\mathbf{1^+/1^\bullet}$ and $\mathbf{1^\bullet/1^-}$, over more than 10 cycles where the surface of $\mathbf{H^+1^-}$ crystals in an electrolyte solution show proton dissociation.[8] Unlike the ligand crystal of $\mathbf{H^+1^-}$, the proton dissociation from the crystal surface of both networks did not occur even after the immersion into the electrolyte solution (Figure S12). As a result, both network crystals showed an irreversible reduction peak of the proton ($\mathbf{H^+1^-} \rightleftarrows H^+ + \mathbf{1^-}$, then $H^+ + e^- \rightarrow 1/2H_2$) during the first cycle around −1.5 V (**Cd-1**$_{mono}$) or −1.53 V (**Cd-1**$_{ortho}$). CV measurements of both networks showed that the potential waves changed over the first several cycles.[11] Although the detailed interpretation of the CV

DOI: 10.1021/jacs.5b12355
J. Am. Chem. Soc. 2016, 138, 1776−1779

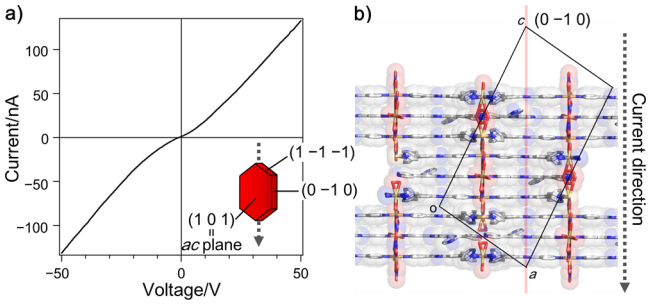

Figure 4. Single crystal electron conductivity of the **Cd-1**$_{mono}$ network. (a) *I*−*V* curve of the single crystal of **Cd-1**$_{mono}$ using the two probe method. Electrical conductivity was measured under ambient conditions (20 ± 1 °C). Inset figure shows the face index of the single crystal. Gray dotted arrow shows the direction of electrode connection. (b) Schematic model of relationship between current direction and TPDAP column direction in **Cd-1**$_{mono}$. Pale red line shows (0 $\bar{1}$ 0) plane.

results is not trivial, we presume that these waves can be assigned as the redox reaction of TPDAP species. Because the ligand has an acidic −NH proton, the potentials of both network crystals were substantially shifted to the cathodic direction compared with those of an $\mathbf{H^+1^-}$ crystal, the surface of which was in deprotonated form in the presence of the electrolyte.[12]

Cd-1$_{mono}$ and **Cd-1**$_{ortho}$ networks showed a significant difference in electrical conductivity, conductor, and insulator, respectively (Figure 4). We expected that a **Cd-1**$_{mono}$ network crystal would show electron conductivity because it possesses unpaired electrons that can move through the network. A two-probe method was used to measure electron conductivity of **Cd-1**$_{mono}$ and **Cd-1**$_{ortho}$ single crystals at 20 ± 1 °C (see Supporting Information). The **Cd-1**$_{mono}$ network crystal showed electron conductivity (~10^{-6} S cm^{-1}) along the π−π stacking column direction (Figure 4a and Table S5), whereas the **Cd-1**$_{ortho}$ network showed no electron conductivity. To reveal the structural contribution to the electron conductivity, we investigated the anisotropic electrical conduction of a **Cd-1**$_{mono}$ network single crystal (Figures 4b and S13): the conductivity was 5 orders of magnitude higher along the π−π stacking column direction than perpendicular to it. These results clearly indicated that the π−π stacking column of the network provided an electron conduction path. Although we have not succeeded in preparing the network using pure $\mathbf{1^\bullet}$ instead of **1**$_{ox}$, we confirmed that after being left for several months **Cd-1**$_{mono}$ showed higher conductivity (~10^{-1} S cm^{-1}) than as-prepared **Cd-1**$_{mono}$ (Figure S14). The temperature-dependent conductivity measurement was performed to investigate the detail mechanism (Figure S15). However, because of deterioration of crystallinity during measurement, we could not obtain the conductivity values clearly. We assume that the increase in conductivity is caused by the increase of the spin amount by further oxidation, although the detailed change in spin is not known.

Finally, we investigated the selective formation of **Cd-1**$_{mono}$ and **Cd-1**$_{ortho}$ depending on the presence or absence of $\mathbf{1^\bullet}$; to generate **Cd-1**$_{mono}$, **1**$_{ox}$ is essential, but in the absence of **1**$_{ox}$, **Cd-1**$_{ortho}$ was always obtained. Therefore, after all $\mathbf{1^\bullet}$ were consumed for **Cd-1**$_{mono}$ formation, **Cd-1**$_{ortho}$ started to crystallize. This fact indicates that $\mathbf{H^+1^-}$ is not oxidized in CH_3OH even under air. We examined time-dependent UV−vis measurements of $\mathbf{H^+1^-}$ and **1**$_{ox}$ in CH_3OH. The result showed the salient difference: an $\mathbf{H^+1^-}$ solution did not show any spectral change in air for a week, whereas the **1**$_{ox}$ solution showed a clear spectral change (Figure S16). In the UV−vis spectra of the **1**$_{ox}$ in air, two bands at 263 and 378 nm attributable to $\mathbf{H^+1^-}$ decreased; concurrently a new band appeared at ~420 nm over several days. However, in the absence of air, no spectral change occurred (Figure S17). Because the 420 nm band was also observed in a day after the preparation of $\mathbf{1^\bullet}$−CH_3OH solution, this band may be originated from the formation of $\mathbf{1^\bullet}$−$\mathbf{1^\bullet}$ dimer (Figure S18). To check the effect of the presence of $\mathbf{1^\bullet}$, we also performed UV−vis measurement of a mixture of $\mathbf{H^+1^-}$ and $\mathbf{1^\bullet}$; it showed similar spectral changes at 420 nm to those observed in **1**$_{ox}$ (Figure S19). ESR experiments also provided the consistent results with the UV data. Especially, the increase of signal intensity demonstrates that O_2-caused further oxidation of $\mathbf{H^+1^-}$ in the presence of $\mathbf{1^\bullet}$ species (Figures S20b,c), whereas no signal was observed in the absence of $\mathbf{1^\bullet}$ (Figure S20a). The oxidation product in **1**$_{ox}$ solution was characterized by ESI-MS and ^{1}H NMR (Figures S3 and S21). ESI-MS of the **1**$_{ox}$ solution left for a week showed two distinct peaks in negative mode; these peaks at *m*/*z* 398 and 795 correspond to $\mathbf{H^+1^-}$ and the $\mathbf{1^\bullet}$−$\mathbf{1^\bullet}$ dimer, respectively. Indeed, VT-^{1}H NMR of **1**$_{ox}$ in CD_3OD is evidence that the $\mathbf{1^\bullet}$−$\mathbf{1^\bullet}$ dimer is present: an NMR spectrum at 253 K showed several broad signals that can be assigned to protons on the DAP skeleton and pyridine rings in the $\mathbf{1^\bullet}$−$\mathbf{1^\bullet}$ dimer.[8,13] Together, these experimental results lead to the conclusion that even a trace amount of $\mathbf{1^\bullet}$ accelerates the further oxidation of $\mathbf{H^+1^-}$ to give $\mathbf{1^\bullet}$−$\mathbf{1^\bullet}$ dimer. Therefore, a plausible reaction mechanism of **1**$_{ox}$ in CH_3OH is as follows: (1) surface oxidation of $\mathbf{H^+1^-}$ crystal in which effective π-stacking of $\mathbf{H^+1^-}$ was formed generates TPDAP radical $\mathbf{1^\bullet}$; (2) in CH_3OH, $\mathbf{1^\bullet}$ and $\mathbf{H^+1^-}$ form $\mathbf{1^\bullet}\cdots\mathbf{H^+1^-}$ dimer that can increase HOMO level of $\mathbf{H^+1^-}$ moiety;[14] (3) oxidation of $\mathbf{H^+1^-}$ moiety in the dimer is caused by O_2;[15] and (4) the amount of $\mathbf{1^\bullet}$ species increases in the solution. In addition, the nonlinear change of dimer intensity in UV−vis spectra of **1**$_{ox}$ (Figure S16b, inset) indicates that newly formed radical $\mathbf{1^\bullet}$ also caused further oxidation of $\mathbf{H^+1^-}$ because the increase of ESR intensity of **1**$_{ox}$ after 215 min exposure in air is more than three times higher than that of after 10 min exposure without any change in *g*-value or line shape change, or formation of new signal. This corresponds to the increase in spin amount of **Cd-1**$_{mono}$ on the basis of the total number of radicals in **1**$_{ox}$. In addition, partial intercalation of radical species can reduce the electric repulsion within the π−π stacking structure. These contributions of $\mathbf{1^\bullet}$ likely induced formation of a conductive columnar structure in the **Cd-1**$_{mono}$ network because it had shorter π−π stacking distance (average 3.3 Å) between DAP skeletons than did **Cd-1**$_{ortho}$.

In summary, we selectively prepared Cd-based conductive/nonconductive coordination networks based on redox active ligand TPDAP by controlling the amount of the radical species $\mathbf{1^\bullet}$. In the absence of $\mathbf{1^\bullet}$, a nonconductive network that has a slipped stacking structure (**Cd-1**$_{ortho}$ network) formed. In contrast, a conductive network that has a columnar structure composed of $\mathbf{H^+1^-}$ with a trace of $\mathbf{1^\bullet}$ (**Cd-1**$_{mono}$ network) was prepared by using surface-oxidized **1**$_{ox}$ crystals. The experimental results indicated that selective network formation dependent on the amount of $\mathbf{1^\bullet}$ was realized by the formation of $\mathbf{H^+1^-}$−$\mathbf{1^\bullet}$ π-dimer (which was generated only in the presence of $\mathbf{1^\bullet}$) followed by further oxidation of $\mathbf{H^+1^-}$.

■ ASSOCIATED CONTENT

Supporting Information

The Supporting Information is available free of charge on the ACS Publications website at DOI: 10.1021/jacs.5b12355.

DOI: 10.1021/jacs.5b12355
J. Am. Chem. Soc. 2016, 138, 1776−1779

Complete data for **Cd-1**$_{mono}$ (CIF)
Complete data for **Cd-1**$_{ortho}$ (CIF)
Details on the experimental procedures, synthesis of Cd^{2+} networks, and supplemental figures (PDF)

AUTHOR INFORMATION

Corresponding Authors

*mkawano@postech.ac.kr
*yakiyama@postech.ac.kr

Present Addresses

[⊥]Department of Applied Chemistry, Graduate School of Engineering, Osaka University, 2-1 Yamadaoka, Suita, Osaka 565-0871, Japan. E-mail: yakiyama@chem.eng.osaka-u.ac.jp.
[#]Department of Chemistry, Graduate School of Science and Engineering, Tokyo Institute of Technology, 2-12-1 Ookayama, Meguro-ku, Tokyo 152-8550, Japan. E-mail: mkawano@chem.titech.ac.jp.

Notes

The authors declare no competing financial interest.

ACKNOWLEDGMENTS

The authors acknowledge funding from the Veteran researcher grant (No. 2014R1A2A1A11049978) and the framework of international cooperation program (No. 2014K2A2A4001500) managed by National Research Foundation of Korea (NRF). This work has been approved by the Photon Factory Advisory Committee (Proposal No. 2014G008, beamline NW2A). Single crystal X-ray diffraction studies with synchrotron radiation were performed at the Pohang Accelerator Laboratory (Beamline 2D). The authors thank Dr. Murata. T. (Aichi Institute of Technology) for fruitful discussion.

REFERENCES

(1) (a) Eddaoudi, M.; Moler, D.; Li, H.; Chen, B.; Reineke, T. M.; O'Keeffe, M.; Yaghi, O. M. *Acc. Chem. Res.* **2001**, *34*, 319−330. (b) Kitagawa, S.; Kitaura, R.; Noro, S.-I. *Angew. Chem., Int. Ed.* **2004**, *43*, 2334−2375. (c) Férey, G. *Chem. Soc. Rev.* **2008**, *37*, 191−214. (d) Robson, R. *Dalton Trans.* **2008**, *38*, 5101−5248. (e) Farha, O. K.; Hupp, J. T. *Acc. Chem. Res.* **2010**, *43*, 1166−1175. (f) Cook, T. R.; Zheng, Y.-R.; Stang, P. J. *Chem. Rev.* **2013**, *113*, 734−777. (g) Furukawa, H.; Cordova, K. E.; O'Keeffe, M.; Yaghi, O. M. *Science* **2013**, *341*, 1230444.

(2) (a) Seo, J. S.; Whang, D.; Lee, H.; Jun, S. I.; Oh, J.; Jeon, Y. J.; Kim, K. *Nature* **2000**, *44*, 982−986. (b) Lee, J.; Farha, O. K.; Roberts, J.; Scheidt, K. A.; Nguyan, S. T.; Hupp, J. T. *Chem. Soc. Rev.* **2009**, *38*, 1450−1459. (c) Farrusseng, D.; Aguado, S.; Pinel, C. *Angew. Chem., Int. Ed.* **2009**, *48*, 7502−7513. (d) Corma, A.; García, H.; Llabrés, I.; Xamena, F. X. *Chem. Rev.* **2010**, *110*, 4606−4655. (e) Jahan, M.; Bao, Q.; Loh, K. *J. Am. Chem. Soc.* **2012**, *134*, 6707−6713. (f) Wang, J.; Wang, C.; Lin, W. *ACS Catal.* **2012**, *2*, 2630−2640.

(3) (a) Feng, D.; G, Z.; Li, J.; Jiang, H.; Wei, Z.; Zhou, H. *Angew. Chem., Int. Ed.* **2012**, *51*, 10307−10310. (b) Ai, L.; Li, L.; Zhang, C.; Fu, J.; Jiang, J. *Chem. - Eur. J.* **2013**, *19*, 15105−15108. (c) Zhang, J.; Zhang, H.; Du, Z.; Wang, X.; Yu, S.; Jiang, H. *Chem. Commun.* **2014**, *50*, 1092−1094. (d) Li, B.; Chen, D.; Wang, J.; Yan, Z.; Jiang, L.; Duan, D.; He, J.; Luo, Z.; Zhang, J.; Yuan, F. *Sci. Rep.* **2014**, *4*, 6759.

(4) (a) Moon, H. R.; Kim, J. H.; Suh, M. P. *Angew. Chem., Int. Ed.* **2005**, *44*, 1261−1265. (b) Bloch, E. D.; Murray, L. J.; Queen, W. L.; Chavan, S.; Maximoff, S. N.; Bigi, J. P.; Krishna, R.; Peterson, V. K.; Grandjean, F.; Long, G. J.; Smit, B.; Bordiga, S.; Brown, C. M.; Long, J. R. *J. Am. Chem. Soc.* **2011**, *133*, 14814−14822. (c) Horike, S.; Sugimoto, M.; Kongpatpanich, K.; Hijikata, Y.; Inukai, M.; Umeyama, D.; Kitao, S.; Seto, M.; Kitagawa, S. *J. Mater. Chem. A* **2013**, *1*, 3675−3679. (d) Leong, C. F.; Faust, T. B.; Turner, P.; Usov, P. M.; Kepart, C. J.; Babarao, R.; Thornton, A. W.; D'Alessandro, D. M. *Dalton Trans.* **2013**, *42*, 9831−9839.

(5) (a) MasPoch, D.; Ruiz-Molina, D.; Wurst, K.; Domingo, N.; Cavallini, M.; Biscarini, F.; Tejada, J.; Rovira, C.; Veciana, J. *Nat. Mater.* **2003**, *2*, 190−195. (b) Maspoch, D.; Ruiz-Molina, D.; Wurst, K.; Rovira, C.; Veciana, J. *Chem. Commun.* **2004**, 1164−1165. (c) Maspoch, D.; Domingo, N.; Molina, D. R.; Wurst, K.; Hernandez, J. M.; Vaughan, G.; Rovira, C.; Lloret, F.; Tejada, J.; Veciana, J. *Chem. Commun.* **2005**, 5035−5037. (d) Alvero, M.; Carbonell, E.; Ferrer, B.; Llabrés i Xamena, F. X.; Garcia, H. *Chem. - Eur. J.* **2007**, *13*, 5106−5112. (e) Takaishi, S.; Hosoda, M.; Kajiwara, T.; Miyasaka, H.; Yamashita, M.; Nakanishi, Y.; Kitagawa, Y.; Yamaguchi, K.; Kobayashi, A.; Kitagawa, H. *Inorg. Chem.* **2009**, *48*, 9048−9050. (f) Narayan, T. C.; Miyakai, T.; Seki, S.; Dincă, M. *J. Am. Chem. Soc.* **2012**, *134*, 12932−12935. (g) Coronado, E.; Minguez Espallargas, G. *Chem. Soc. Rev.* **2013**, *42*, 1525−1539. (h) Talin, A. A.; Centrone, A.; Ford, A. C.; Foster, M. E.; Stavila, V.; Haney, P.; Kinney, R. A.; Szalai, V.; Gably, F. E.; Yoon, H. P.; Léonard, F.; Allendorf, M. D. *Science* **2014**, *343*, 66−69. (i) Zhang, Z.; Yoshikawa, H.; Awaga, K. *J. Am. Chem. Soc.* **2014**, *136*, 16112−16115.

(6) (a) Roques, N.; Maspoch, D.; Domingo, N.; Ruiz-Molina, D.; Wurst, K.; Tejada, J.; Rovira, C.; Veciana, J. *Chem. Commun.* **2005**, 4801−4803. (b) Alley, K. G.; Poneti, G.; Aitken, J. B.; Hocking, P. K.; Moubaraki, B.; Murray, K. S.; Abrahams, B. F.; Harris, H. H.; Sorace, L.; Boskovic, C. *Inorg. Chem.* **2012**, *51*, 3944−3946. (c) Alley, K. G.; Poneti, G.; Robinson, P. S. D.; Nafady, A.; Moubaraki, B.; Aitken, J. B.; Drew, S. C.; Ritchie, C.; Abrahams, B. F.; Hocking, R. K.; Murray, K. S.; Bond, A. M.; Harris, H. H.; Sorace, L.; Boskovic, C. *J. Am. Chem. Soc.* **2013**, *135*, 8304−8323. (d) Faust, T. B.; D'Alessandro, D. M. *RSC Adv.* **2014**, *4*, 17498−17512.

(7) (a) Yakiyama, Y.; Ueda, A.; Morita, Y.; Kawano, M. *Chem. Commun.* **2012**, *48*, 10651−10653. (b) Kojima, T.; Yamada, T.; Yakiyama, Y.; Ishikawa, E.; Morita, Y.; Ebihara, M.; Kawano, M. *CrystEngComm* **2014**, *16*, 6335−6344. (c) Yakiyama, Y.; Lee, G.; Kim, S.; Matsushita, Y.; Morita, Y.; Park, M.; Kawano, M. *Chem. Commun.* **2015**, *51*, 6828−6831. (d) Yakiyama, Y.; Kojima, T.; Kawano, M. Crystal Engineering of Coordination Networks Using Multi-Interactive Ligands. In *Advances in Organic Crystal Chemistry: Comprehensive Reviews 2015*; Tamura, R., Miyata, M., Eds.; Springer: Tokyo, 2015; pp 223−240.

(8) Koo, J. Y.; Yakiyama, Y.; Kim, J.; Morita, Y.; Kawano, M. *Chem. Lett.* **2015**, *44*, 1131−1133.

(9) (a) Morita, Y.; Aoki, T.; Fukui, K.; Nakazawa, S.; Tamaki, K.; Suzuki, S.; Fuyuhiro, A.; Yamamoto, K.; Sato, K.; Shiomi, D.; Naito, A.; Takui, T.; Nakasuji, K. *Angew. Chem., Int. Ed.* **2002**, *41*, 1793−1796. (b) Morita, Y.; Suzuki, S.; Fukui, K.; Nakazawa, S.; Kitagawa, H.; Kishida, H.; Okamoto, H.; Naito, A.; Sekine, A.; Ohashi, Y.; Shiro, M.; Sasaki, K.; Shiomi, D.; Sato, K.; Takui, Y.; Nakasuji, K. *Nat. Mater.* **2008**, *7*, 48−51. (c) Morita, Y.; Suzuki, S.; Sato, K.; Takui, T. *Nat. Chem.* **2011**, *3*, 197−204.

(10) Morita, Y.; Nishida, S.; Murata, T.; Moriguchi, M.; Ueda, A.; Satoh, S.; Arifuku, K.; Sato, K.; Takui, T. *Nat. Mater.* **2011**, *10*, 947−951.

(11) Leong, C. F.; Chan, B.; Faust, T. B.; D'Alessandro, M. D. *Chem. Sci.* **2014**, *5*, 4724−4728.

(12) McCarthy, B. D.; Martin, D. J.; Rountree, E. S.; Ullman, A. C.; Dempsey, J. L. *Inorg. Chem.* **2014**, *53*, 8350−8361.

(13) Mou, Z.; Uchida, K.; Kubo, T.; Kertesz, M. *J. Am. Chem. Soc.* **2014**, *136*, 18009−18022.

(14) Kochi, J. K.; et al. reported the formation of dimer between the closed-shell species and its radical especially in the phenalenyl system. See (a) Small, D.; Zaitsev, V.; Jung, Y.; Rosokha, S. V.; Head-Gordon, M.; Kochi, J. K. *J. Am. Chem. Soc.* **2004**, *126*, 13850−13858. (b) Small, D.; Rosokha, S. V.; Kochi, J. K.; Head-Gordon, M. *J. Phys. Chem. A* **2005**, *109*, 11261−11267.

(15) (a) Nandwana, V.; Samuel, I.; Cooke, G.; Rotello, V. M. *Acc. Chem. Res.* **2013**, *46*, 1000−1009. (b) Bravaya, K. B.; Kostko, O.; Ahmed, M.; Krylov, A. I. *Phys. Chem. Chem. Phys.* **2010**, *12*, 2292−2307.

DOI: 10.1021/jacs.5b12355
J. Am. Chem. Soc. 2016, 138, 1776−1779